

Numerical study of the negative nonlocal resistance and the backflow current in a ballistic graphene system

Zibo Wang,^{1,2} Haiwen Liu,³ Hua Jiang,^{4,5,*} and X. C. Xie^{6,7,8}

¹Microsystem and Terahertz Research Center, China Academy of Engineering Physics, Chengdu 610200, China

²Institute of Electronic Engineering, China Academy of Engineering Physics, Mianyang 621999, China

³Center for Advanced Quantum Studies, Department of Physics,
Beijing Normal University, Beijing 100875, China

⁴School of Physical Science and Technology, Soochow University, Suzhou 215006, China

⁵Institute for Advanced Study of Soochow University, Suzhou 215006, China

⁶International Center for Quantum Materials, School of Physics, Peking University, Beijing 100871, China

⁷CAS Center for Excellence in Topological Quantum Computation,
University of Chinese Academy of Sciences, Beijing 100190, China

⁸Beijing Academy of Quantum Information Sciences, West Bld.3,
No.10 Xibeiwang East Rd., Haidian District, Beijing 100193, China

(Dated: October 10, 2019)

Besides the giant peak of the nonlocal resistance R_{NL} , an anomalous negative value of R_{NL} has been observed in graphene systems, while its formation mechanism is not quite understood yet. In this work, utilizing the non-equilibrium Green's function method, we calculate the local-current flow in an H-shaped non-interacting graphene system locating in the ballistic regime. Similar to the previous conclusions made from the viscous hydrodynamics, the numerical results show that a local-current vortex appears between the nonlocal measuring terminals, which induces a backflow current and a remarkable negative voltage drop at the probe. Specifically, the stronger the vortex exhibits, the more negative R_{NL} manifests. Besides, a spin-orbital coupling is added as an additional tool to study this exotic vortex, which is not a driving force for the arising vortex at all. Moreover, a breakdown of the nonlocal Wiedemann-Franz law is obtained in this ballistic system, and two experimental criteria are further provided to confirm the existence of this exotic vortex. Notably, a discussion is made that the vortex actually originates from the collision between the flowing current and the boundaries, due to the long electron mean free path and the consequent ballistic transport caused by the specific linear spectrum of graphene.

PACS numbers: 71.70.Ej, 72.10.-d, 73.23.-b

I. INTRODUCTION

Nonlocal measurement indicates the detection of a voltage signal away from the path that the current is expected to follow, and has been developed as a powerful tool to discover nontrivial interactions difficult to detect directly, such as the electron-electron (ee) interaction, viscosity, spin-orbital coupling, etc¹⁻¹³. Besides the giant peak of the nonlocal resistance R_{NL} , more and more experiments have observed an anomalous negative value of the nonlocal resistance^{9,10,13}, which means the local current close to the nonlocal terminals flows in direction opposite to the injected current. Till now, kinds of theories have been proposed to explain this exotic phenomenon, such as the viscous hydrodynamic fluid^{9,14-16}, the ballistic transport¹⁷⁻²⁰, the magnetoelectric coupling²¹ and so on.

Among these theories, viscous hydrodynamics is the most developed one^{9,14-16}, and has been supported by the recent experiments for a two-dimensional fluid of electrons in graphene^{13,22}. The condition for viscous hydrodynamics happens when the extrinsic scattering length r is far greater than the ee collision mean free path l_{ee} . That is to say, electrons injected into the system must undergo frequent collisions with each other inside the bulk, which can be well described by the theory of

hydrodynamics²³⁻²⁵. For instance, Bandurin et al. detected an anomalous nonlocal negative voltage drop in a multi-terminal graphene device on the order of $1\mu m$ ⁹. By solving the hydrodynamic equations, a submicrometer-size whirlpool in the electron flow can be obtained. Moreover, the calculation results show that the whirlpool enhances with the increase of the viscosity, and disappears with zero viscosity, which fits the experiment well. Thus, this negative nonlocal resistance is attributed to the formation of a local-current vortex.

More comprehensively, some literatures further propose that in the ee interaction dominated but quasi-ballistic regime, where r is much smaller than l_{ee} , the negative value of the nonlocal resistance can occur as well^{10,11,17}. Furthermore, as a direct prove to the ballistic transport without ee collision, our previous work and others based on the non-equilibrium Green's function (NEGF) method predict that the ballistic transport itself could induce a negative nonlocal resistance^{18,19}. In addition, with the help of the semi-classical Boltzmann equation and phenomenological conditions, recent work could even obtain a vortex in the ballistic regime classically²⁰. However, compared with the well-studied theory in hydrodynamics, the formation mechanism of the negative R_{NL} observed in ballistic system without ee interaction desperately needs in-depth analysis, such as the demon-

stration of the local-current flow in the view of quantum transport.

In this work, we further study the origin of the negative nonlocal resistance in a non-interacting graphene model with an external Rashba effect, and try to confirm whether the local-current vortex also exists in this ballistic system, similar as that in a viscous fluid⁹. First, in an H-shaped four-terminal graphene system, we calculate the local-current distribution with different Fermi energy E_F and different Rashba strength λ_R . The results show that an exotic vortex emerges between the two nonlocal measuring terminals similar to that in a viscous fluid. Further calculation indicates that this vortex strengthens with the decrease of λ_R . In comparison with the fact that the negative value of the nonlocal resistance also increases with weakening Rashba effect, we confirm that the vortex has a positive relation to the negative nonlocal resistance. Thus, a conclusion can be made that the ballistic transport in the nonlocal measurement does exist in the form of a vortex, which consists of backflow current and induces a negative contribution to the nonlocal resistance. Then, the local and nonlocal thermal conductance of this system are also obtained within the NEGF framework. In comparison to the scaled local (nonlocal) electrical conductance $\mathcal{L}_0^{-1}R_L/T$ ($\mathcal{L}_0^{-1}R_{NL}/T$), we find that our ballistic system actually breaks the nonlocal Wiedemann-Franz (WF) law instead of the local one found in hydrodynamics²⁶, and this violation gradually disappears with weakening vortex strength. Based on the above results, we further propose two experimental methods to confirm the existence of the local-current vortex in a ballistic system. Specifically, with increasing λ_R , both the negative value of R_{NL} and the breakdown of the nonlocal WF law should gradually disappear in ballistic regime. At last, a discussion is made that it is actually the collision between the flowing current and the boundaries that induces this exotic vortex. Since this collision highly relies on a long electron mean free path l_e and the consequent ballistic transport, the vortex will be much easier to be observed in graphene due to its unique linear energy dispersion.

The rest of this paper is organized as follows. In Sec.II, we first numerically obtain the local-current flow and find a vortex in an H-shaped four-terminal ballistic graphene system. Then, in Sec.III, we propose two experimentally feasible methods to confirm the existence of this vortex indirectly in the ballistic regime. Next, a discussion about the possible origin of the vortex flow is made in Sec.IV. And finally, a conclusion is presented in Sec.V.

II. LOCAL-CURRENT FLOW IN H-SHAPED FOUR-TERMINAL SYSTEM

In this work, we consider an H-shaped four-terminal graphene system²⁷, whose schematic diagram is shown in Fig.1(a), to simulate the local current distribution in the nonlocal measuring experiment. The central re-

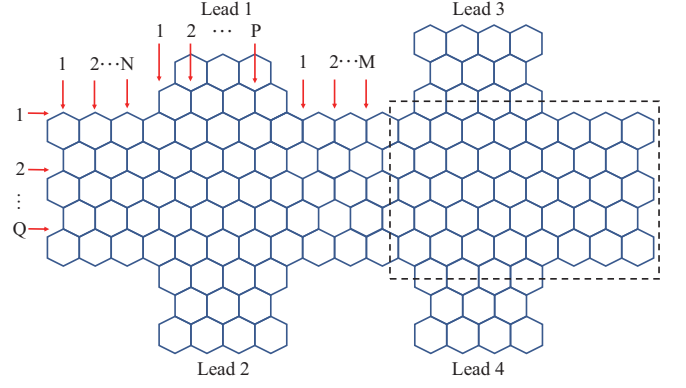


FIG. 1: The schematic diagram of the H-shaped four-terminal system. The current is injected from lead 1 to lead 2. The voltage signal is detected on lead 12 for the local resistance, and on lead 34 for the nonlocal resistance. The rectangle circled by the black dashed line indicates the region where the local-current flow is calculated.

gion for this system is marked with parameters M, N, P and Q . For instance, in Fig.1, we show a sample with $M = N = Q = 3$ and $P = 4$. During the calculation process, the current is injected from lead 1 and flows out from lead 2. Meanwhile, the nonlocal voltage is detected between lead 3 and 4. In this paper, we only show the local current distributed in the rectangle region, which is surrounded by the black dashed line. This is due to the fact that we find the local-current flow exhibits nontrivial characteristics only between the nonlocal measuring terminals, and exhibits the classical Ohmic distribution in other regions.

Similar as our previous work of Ref.[18], the tight-binding Hamiltonian for this system is written as:

$$H = \sum_i \epsilon_i c_i^\dagger c_i - t \sum_{\langle ij \rangle} c_i^\dagger c_j + i\lambda_R \sum_{\langle ij \rangle} c_i^\dagger (\mathbf{s} \times \hat{\mathbf{d}}_{ij})_z c_j. \quad (1)$$

The first term is the on-site potential with ϵ_i on the i th carbon atom. The second term represents the nearest-neighbor hopping with strength t . In the following calculation, we take t as the energy unit and all other parameters are normalized based on $t = 2.8\text{eV}$. The last term describes the external Rashba effect with strength λ_R . The disorder existing in the central region is modeled by Anderson disorder with random potential uniformly distributed in $[-w/2, w/2]$, where w is the disorder strength. In this work, we choose $w = 1$.

In Ref.[18], we have specifically introduced how to calculate the local and the nonlocal resistance: $R_L = (V_1 - V_2)/I_1$ and $R_{NL} = (V_3 - V_4)/I_1$ based on the Landauer-Buttiker formula³¹. Since it's the local-current distribution that we focus on in this work, the size of the central region is limited for the convenience and clearness to read the local-current flow vectors inside the black dashed line. Thus, the size parameters M, N, P and Q are chosen as $M = 10, N = 5, P = 20$ and $Q = 20$, which means the size of this system we calculated is about

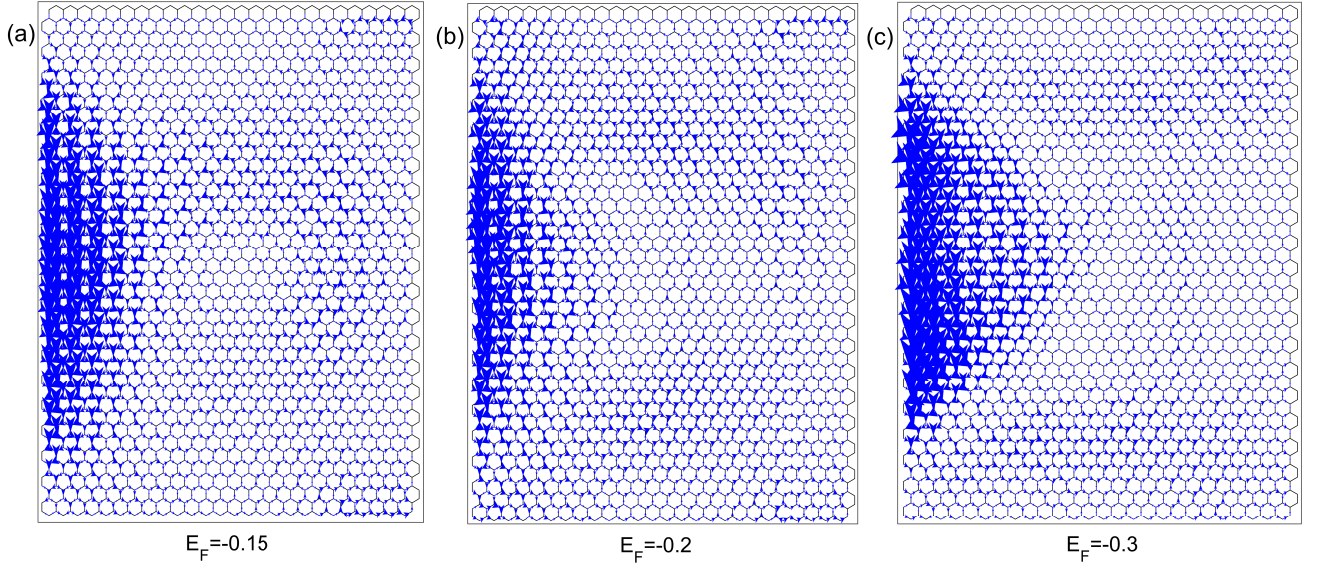


FIG. 2: The local current flow in the black dashed rectangle marked in Fig.1 when $\lambda_R = 0.1$. (a) $E_F = -0.15$; (b) $E_F = -0.2$; (c) $E_F = -0.3$. The size of each arrow is proportional to the strength of the local current vector. It is obvious that a counter-clockwise vortex emerges in panel (a) and gradually disappears with the increase of $|E_F|$ in panels (b) and (c). All three panels have sufficiently high resolutions to be zoomed in to show the vortex clearly.

$20nm \times 10nm^{28}$.

In order to simulate the local-current flow in the non-local measuring experiment, a small external voltage bias $V = V_1 - V_2$ is applied between lead 1 and 2. With the help of the NEGF method, the local current flows from site i to its neighbor j can be deduced as^{29,30}:

$$J_{i \rightarrow j} = -\frac{2e}{h} \sum_{\alpha, \beta} \int_{-\infty}^{\infty} dE \text{Re}[H_{i\alpha, j\beta} G_{j\beta, i\alpha}^K(E)], \quad (2)$$

where α, β denote the spin indices, and $G_{j\beta, i\alpha}^K(E)$ is the Keldysh Green's function. When the applied voltage $V_{1,2}$ is small and the system is in the zero temperature, by applying the Keldysh equation $G^K = G^r \sum_n i\Gamma_n f_n G^a$ and assuming $V_1 > V_2$, the Eq.(2) can be rewritten as:

$$J_{i \rightarrow j} = \frac{2e}{h} \sum_{\alpha, \beta} \int_{-\infty}^{eV_2} dE \text{Im}\{H_{i\alpha, j\beta} [G^r \sum_n \Gamma_n G^a]_{j\beta, i\alpha}\} + \frac{2e^2}{h} \sum_{\alpha, \beta} \text{Im}[H_{i\alpha, j\beta} \sum_n G_{j\beta, i\alpha}^n(E_F)(V_n - V_2)] \quad (3)$$

where V_n is the voltage of the n th lead, and can be obtained in the calculation of R_{NL} . $G^n(E) = G^r(E)\Gamma_n(E)G^a(E)$ is the electron correlation function. The linewidth function is $\Gamma_n(E) = i\{\Sigma_n^r(E) - [\Sigma_n^r(E)]^\dagger\}$, and the Green's function reads $G^r(E) = [G^a(E)]^\dagger = [EI - H_{cen} - \sum_n \Sigma_n^r(E)]$. Here, $\Sigma_n^r(E)$ is the retarded self-energy due to the coupling to the n th lead, and H_{cen} is the Hamiltonian used in the central region. The first part of Eq.(3) gives rise to the equilibrium current \mathbf{J}_{eq} , which equals zero due to the time-reversal symmetry of the Hamiltonian described by Eq.(1). Thus, the local

current flows from site i to its neighbor j can be simplified as:

$$J_{i \rightarrow j} = \frac{2e^2}{h} \text{Im} \sum_{\alpha, \beta} [H_{i\alpha, j\beta} \sum_n G_{j\beta, i\alpha}^n(E_F)(V_n - V_2)]. \quad (4)$$

Moreover, based on Eq.(4), the current I_n flowing from lead n to the central region can be obtained by summing over all the local current $\sum_i J_{i, i+\delta y}$ at the boundary between lead n and the central region. In comparison with I_n acquired from the previous calculation of R_L and R_{NL} , we can further testify the correctness of Eq.(4) and the accuracy of our calculation program.

In Fig.2, we first show the spatial distributions of the local current inside the black dashed rectangle marked in Fig.1, when the Rashba effect is fixed at $\lambda_R = 0.1$. Throughout this work, we only discuss the negative part of the Fermi energy E_F for simplicity, and the conclusion for positive E_F is the same. From Fig.2(a) to 2(c), the Fermi energy locates at $E_F = -0.15, -0.2$ and -0.3 , respectively. Here, the size and the orientation of the arrows indicate the strength and the direction of the local-current flow.

As shown in Fig.2(a), it is obvious that there exists a counter-clockwise vortex of the local current between the two nonlocal measuring terminals³², which seems like the whirlpools obtained in viscous hydrodynamic systems. Importantly, the appearance of this vortex induces a kind of backflow current flowing from lead 4 to lead 3, which is in the direction opposite to the injected current. Consequently, there exists a competition between the positive voltage drop caused by the Ohmic transport and the negative one caused by the backflow current. Thus, it is natural for us to anticipate that if the “vortex strength”³³ is

strong enough, a negative voltage drop between V_3 and V_4 will be detected, and a negative nonlocal resistance R_{NL} will be obtained consequently as people have shown in previous work.

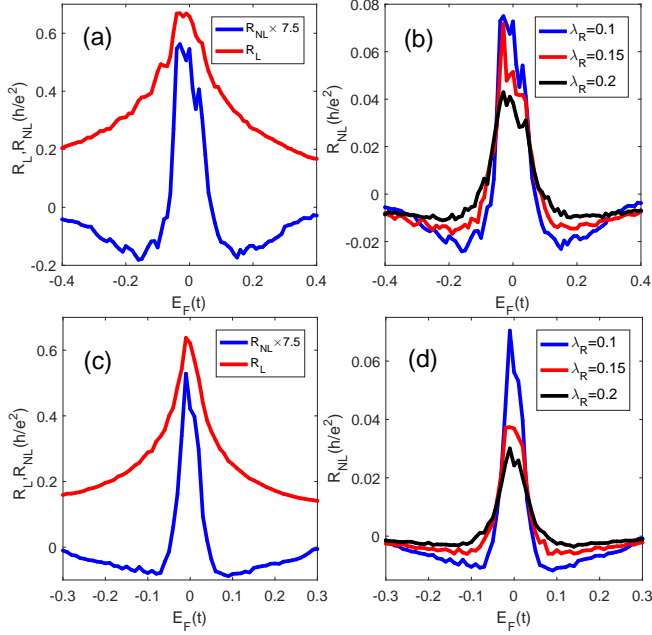


FIG. 3: (a) The local resistance R_L (red) and nonlocal resistance R_{NL} (blue) when $\lambda_R = 0.1$. (b) The nonlocal resistance R_{NL} with different Rashba strengths. The negative peak of R_{NL} reaches its maximum at $\lambda_R = 0.1$ (blue), and gradually decreases with the increase of λ_R (red and black). (c) and (d) The same results of panels (a) and (b) with double size parameters, where the oscillations seem not evident now.

Moreover, from Fig.2(a) to 2(c), we find that the strength of the vortex reaches its maximum at $E_F = -0.15$, then weakens gradually with the increase of the Fermi energy, and finally disappears when the Fermi energy is large enough. In order to confirm the relationship between the vortex of the local current and the appearance of the negative R_{NL} , in Fig.3(a), we show how R_L and R_{NL} vary with the Fermi energy E_F when the Rashba effect is fixed at $\lambda_R = 0.1$. The macroscopic oscillations come from the resonance in the Fabry-Pérot cavity, because the size of our system is very small. As a contrast, in Fig.3(c) and 3(d), we show the result with a system twice the size of that in Fig.3(a) and 3(b), where the oscillations become relatively negligible now. Notably, in Fig.3(c) and 3(d), we find the whole shape of R_{NL} vs E_F shrinks along the E_F axis and the negative peak move towards the original point. Since the Rashba effect always appears in the form of λ_R/E_F during the calculation, the shrink of E_F indicates that a smaller λ_R is needed with a larger system size, which is more practical in experiments. In Fig.3(a), it is obvious that the blue lines of R_{NL} exhibits a giant peak near the Dirac point, then decays rapidly to its negative maximum at about $E_F = -0.15$, and finally approaches zero

as the absolute value of E_F continues to increase. The giant peak of R_{NL} has been discussed in our previous work¹⁸, which is assumed resulting from the extremely small density of states at the Dirac point, and has no relationship to the vortex in our system. Thus, in order to eliminate this effect, we only consider the region where $E_F < -0.15$ throughout this work. As expected, by comparing Fig.2 and Fig.3(a), the most negative R_{NL} locates exactly where the strongest vortex emerges, and the negative value of R_{NL} decreases as the vortex disappears gradually. Thus, we can make a conclusion that the negative value of R_{NL} originates from the vortex emerging between the nonlocal measuring terminals. The stronger the vortex exhibits, the more negative R_{NL} manifests.

Another method to further study the relationship between the negative value of R_{NL} and the strength of the vortex is to alter the Rashba strength λ_R while E_F remains unchanged. In Fig.3(b), we show how R_{NL} varies with E_F under three different Rashba strengths $\lambda_R = 0.1, 0.15$ and 0.2 . As one can see, apart from the region close to the Dirac point, the negative value of R_{NL} decreases with increasing λ_R . This phenomenon can be understood as follows: if the Rashba effect is extremely strong, the current injected into lead 1 will first transport to lead 3 along the upper edge of the system due to the spin Hall effect, then undergoes collisions with the boundary of the system, and finally flows from lead 3 to lead 4. As above, the Rashba effect actually makes a positive contribution to the nonlocal resistance R_{NL} , which is in consistent with our previous calculation of R_{Hall} shown in Ref.[18]. However, since the Rashba effect and the vortex always coexist with each other in reality, the local-current flow induced by the Rashba effect will eliminate the strength of the vortex caused by the ballistic transport in a certain degree. Consequently, the vortex should gradually disappear as the Rashba effect strengthens.

Following this line of reasoning, in Fig.4, we show the spatial distributions of the local current inside the black dashed rectangle marked in Fig.1, when the Fermi energy is fixed at $E_F = -0.15$. From Fig.4(a) to 4(c), the strength of the Rashba effect increases from $\lambda_R = 0.1$ to 0.15 and 0.2 . As expected before, the vortex exhibits most obviously at $\lambda_R = 0.1$, and gradually disappears with the increase of λ_R . Now, based on the calculation of the local-current flow, we demonstrate that the ballistic transport proposed in previous works indeed gives rise to a vortex in the local-current distribution, which further induces backflow current in the direction opposite to the injected current and results in the negative R_{NL} observed both in theory and experiment. Specifically, the stronger the vortex is, the more negative R_{NL} exhibits.

III. TWO EXPERIMENTAL CRITERIA TO THE EXISTENCE OF THE BACKFLOW CURRENT

Interestingly, the backflow current induced by the vortex shown in Fig.2 and 4 has also been obtained theoretic-

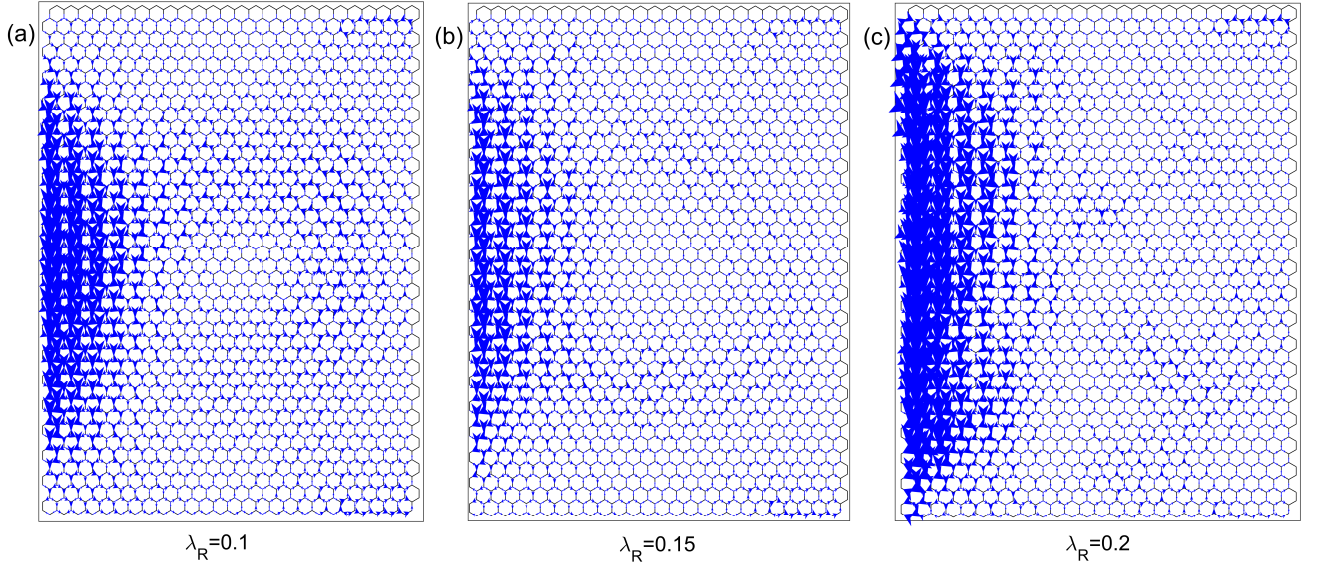


FIG. 4: The local current flow in the black dashed rectangle marked in Fig.1 when E_F is fixed at -0.15. From panel (a)-(c), the Rashba strength increases from $\lambda_R = 0.1$ to 0.15 and 0.2, respectively. The size of each arrow is proportional to the strength of the local current vector. We find that the vortex is evident with a smaller Rashba effect, and gradually disappears with the increase of λ_R . Since the vortex in panel (c) is too weak, the size of the arrows in this panel has been strengthened by two times compared with those in panels (a) and (b). All three panels have sufficiently high resolutions to be zoomed in to show the vortex clearly.

cally in graphene system dominated by ee interaction^{9,14}. To be specific, although the Hamiltonian of Eq.(1) has no terms of ee interaction and locates at the ballistic regime, both our system and the ee dominated one described by viscous hydrodynamics exhibit similar properties: the negative value of R_{NL} and the backflow current. Significantly, in hydrodynamic theories, the vortex strength highly depends on the viscosity magnitude, and the vortex disappears with zero viscosity. In contrast, for our ballistic system, according to Fig.4, the vortex strength decreases with the increasing Rashba effect. Thus, the backflow current and the negative value of R_{NL} proposed in our ballistic system can be controlled by tuning the Rashba strength λ_R , which mainly relies on external electric field and can be realized in experiments. Furthermore, since λ_R has little relation to the viscosity, we believe that one possible method to distinguish the appearance of the vortex current between the ballistic and the hydrodynamic system is to tune the external electric field in order to alter the extrinsic Rashba strength λ_R . Specifically, by increasing the external electric field, a reduction of the negative R_{NL} will be detected in experiment, which indicates the weakening of the backflow current in the ballistic regime. While the hydrodynamic regime is not sensitive to the varying Rashba effect.

In addition, there also exist other signatures for the appearance of backflow current in the ballistic regime. For instance, the breakdown of the nonlocal WF law based on the NEGF calculation. The local and nonlocal thermal conductances are defined as: $\Theta_L = (T_1 - T_2)/Q_1$ and $\Theta_{NL} = (T_3 - T_4)/Q_1$, respectively. Here, T_i indicates the

temperature of lead i and Q_i represents the heat current flowing from lead i to the central region. Based on the NEGF method, Q_i can be calculated as³⁴:

$$Q_i = \frac{1}{h} \sum_j \int dE (E - E_F)^2 f_0(1 - f_0) \mathcal{T}_{ij}(E) \frac{T_i - T_j}{k_B T^2}, \quad (5)$$

where $f_0(E) = 1/(1 + \exp \frac{E - E_F}{k_B T})$ is the Fermi distribution function. And $\mathcal{T}_{ij}(E)$ is the transmission coefficient from lead i to j , which can be obtained during the calculation of R_L and R_{NL} .

In Fig.5(a), we first plot the local thermal conductance Θ_L alongside E_F at $T = 500K$ when $\lambda_R = 0.1$. For a direct quantitative comparison based on the WF law, the scaled local conductance $\mathcal{L}_0^{-1} R_L/T$ in the same units as Θ_L is also shown, where $\mathcal{L}_0 = \frac{\pi^2}{3} (\frac{k_B}{e})^2$ is the Lorenz ratio. It is obvious that these two values coincide with each other when the absolute value of E_F is larger than 0.1. Then, in Fig.5(b), we also show the non-local thermal conductance Θ_{NL} and its corresponding scaled nonlocal conductance $\mathcal{L}_0^{-1} R_{NL}/T$. The major difference between Fig.5(a) and 5(b) is that: the latter one exhibits an obviously additional violation of the nonlocal WF law at $-0.3 < E_F < -0.1$, while the former one does not. Moreover, in Fig.5(b), $\mathcal{L}_0^{-1} R_{NL}/T$ is higher than Θ_{NL} near the Dirac point, and this relationship reverses at $-0.3 < E_F < -0.1$. The above phenomena indicate that the physical pictures behind the violations at $-0.3 < E_F < -0.1$ and $-0.1 < E_F < 0.1$ must be totally different. Since the vortex only exists between the nonlocal measuring terminals, which affects the nonlocal

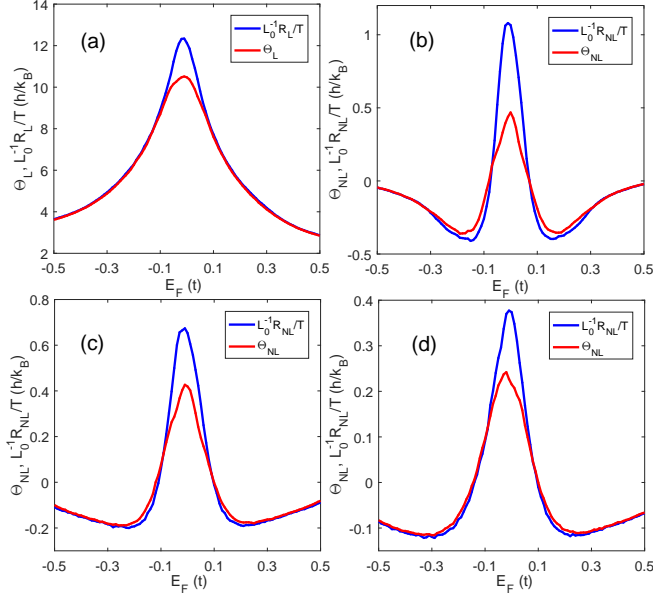


FIG. 5: (a) The local thermal conductance Θ_L (red) as a function of the Fermi energy E_F , compared with the local WF law $\mathcal{L}_0^{-1}R_L/T$ (blue) at $T = 500K$ and $\lambda_R = 0.1$. (b)-(d) The nonlocal thermal conductance Θ_{NL} (red) and the corresponding nonlocal WF law $\mathcal{L}_0^{-1}R_{NL}/T$ (blue) from $\lambda_R = 0.1$ to 0.2 and 0.3 , respectively.

WF law instead of the local one, it is most likely that the violation at $-0.3 < E_F < -0.1$ results from this exotic vortex.

In order to further confirm the origin of the violation at $-0.3 < E_F < -0.1$, we enlarge the Rashba strength from $\lambda_R = 0.1$ to 0.2 and 0.3 in Fig.5(c) and 5(d), respectively. It is clear that the nonlocal WF law breakdown at $-0.3 < E_F < -0.1$ gradually weakens with the increase of λ_R , which provides evidence for the claim that this nonlocal WF law violation actually originates from the vortex and its subsequent backflow current. Thus, it is another feasible method in experiments that the appearance of the vortex in ballistic system could be testified indirectly with the nonlocal thermal conductance and the consequent breakdown of the nonlocal WF law. More accurate analysis for the formation mechanism of this violation needs a comparison between the local electrical current flow and local thermal current flow, which is not shown in this work.

Above all, by altering the Rashba spin-orbital interaction strength λ_R , two possible experimental methods have been proposed to distinguish the appearance of the local-current vortex in ballistic regime. The first one is to detect the negative value of R_{NL} and its variation with λ_R , and the second one is to probe the nonlocal thermal conductance Θ_{NL} and compared it with the nonlocal WF law.

IV. DISCUSSION

In this section, let's focus on the possible mechanisms to the formation of the exotic vortex. First, the effect of the impurity scattering needs to be clarified in our analysis. For comparison, we also calculate R_{NL} under a weaker disorder strength $w = 0.5$ compared with $w = 1$ presented above. However, the calculating results show that R_{NL} with $w = 0.5$ exhibits more negative value than that with $w = 1$. Therefore, the collision between the electrons and the impurities inside actually plays a negative role to the formation of the vortex.

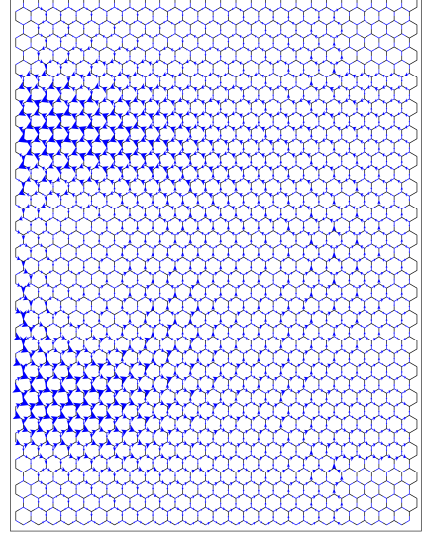


FIG. 6: The local current flow in the black dashed rectangle marked in Fig.1 when a list of very strong Anderson disorder is added at the boundaries, Other parameters are all the same as those in Fig.2(a). It is obvious that a counter-clockwise vortex remains, and tends to move forward into the central region compared with Fig.2(a).

Then, based on the Boltzmann equation, a recently published literature proved that a vortex could also be found in the ballistic regime²⁰. In this semi-classical calculation, the momentum relaxation time is set so small that the system has a sufficient long electron mean free path (l_e) and definitely locates in the ballistic regime. Thus, there must exist collisions between the flowing electrons and the boundaries, which seems like the key role to the observation of the vortex. In Fig.6, by adding a list of very strong Anderson disorder at the boundaries of our model, the boundary condition of the specular reflection can be changed to a diffuse one, which loses momentum but keeps energy conservation. As we can see, there still exists a vortex between the nonlocal measuring terminals. The main difference between Fig.6 and 2(a) is that the vortex in Fig.6 tends to move left into the central region. This phenomenon comes from the fact that the net momentum parallel to the boundary becomes zero after the diffuse scattering, while the net perpendicular momentum still exists. Based on the above analysis, we

believe that the vortex directly originates from the collisions between the injected current and the boundaries, which is the result of ballistic transport and the corresponding long l_e .

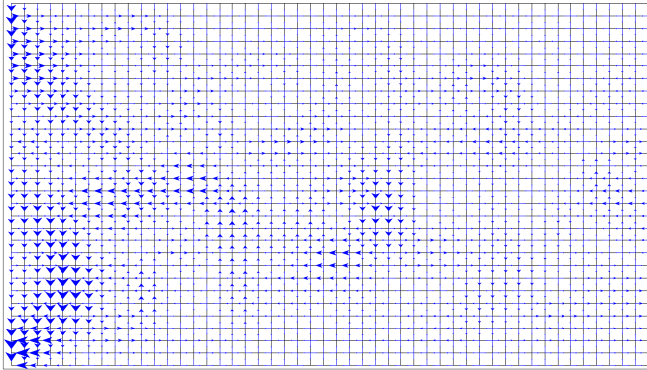


FIG. 7: The local current flow of a square lattice whose size and Hamiltonian are the same as those in Fig.1. It is obvious that no vortex exists any more.

Following the above analysis, the kernel question turns into which condition could guarantee such a long l_e that the system locates in the ballistic regime. In Fig.7, we further calculate the local-current distribution of a square lattice model whose size and Hamiltonian are the same as those of the graphene model used previously. In order to make a better comparison between the graphene and square lattice, the Fermi energy is fixed at $E_F = -3.8t$, which guarantees E_F locates near the bottom band of the square lattice spectrum. Thus, both the energy and the momentum are nearly the same and consequently comparable between the graphene and the square lattice model.

As shown in Fig.7, though the Rashba strength is chosen as $\lambda_R = 0.1$, which is the same as that in Fig.2(a), it is clear that only the classical Ohm-like current could be found and no vortex exists in the square lattice model. This phenomenon comes from the fact that at the small momentum k , both the graphene and the square lattice structures have relatively large wavelength. However, since there exists linear spectrum relationship in honeycomb lattice, graphene is delocalized compared with the strong Anderson localization in square lattice. Thus, l_e in square lattice will be much smaller than that in honeycomb lattice. To a certain degree, when l_e of the square lattice decreases to be shorter than the size of the system, there is no ballistic transport, which results in the disappearance of the vortex in square lattice as shown in Fig.7.

To sum up, we can now make a conclusion that the vortex directly results from the elastic or semi-elastic collision between the injected current and the boundaries. However, this collision needs the existence of a sufficient long l_e and the consequent ballistic transport, which highly relies on the linear spectrum of the graphene and the electron delocalization. Thus, it will be much easier for us to obtain a vortex with a relatively pure

graphene sample than others.

Finally, the difference between the classical Boltzmann equation and our NEGF method should also be clarified. Specifically, the use of the classical Boltzmann equation needs a sufficient long l_e , which is not calculated microscopically but only considered phenomenologically. That is to say, the establishment of the Boltzmann equation depends on the condition that the system has already located in the ballistic regime, which makes no difference to the honeycomb and square lattices. In contrast, our calculation based on the NEGF method originates from the basic Hamiltonian. And the quantum transport could deal with different values of disorder strength, which is more accurate and helps us better understand the specific differences between the honeycomb and square lattice structures.

V. CONCLUSION

In conclusion, using the NEGF method, we first calculate the local-current flow in an H-shaped noninteracting graphene system locating in the ballistic regime. Interestingly, an obvious vortex, similar to the one appears in a viscous hydrodynamic fluid, can be found between the nonlocal measuring terminals. This vortex strengthens with decreasing of the external Rashba effect, and induces a backflow current in the direction opposite to that of the injected current. These properties highly accord with the confusing negative nonlocal resistance R_{NL} , which has been observed in both experiments and theories previously. The consistency comes from the fact that the backflow current results in a negative voltage drop between the nonlocal measuring terminals, and further induces a competition to the positive one caused by the spin Hall transport. Furthermore, we demonstrate that with enlarging Rashba effect strength, both the vortex and the corresponding negative value of R_{NL} become smaller, and disappear simultaneously when the Rashba effect strength is sufficiently strong. Thus, we conclude that the ballistic transport can also give rise to a vortex, and may serve as a different origin of the observed negative nonlocal R_{NL} , providing an alternative picture to that of the viscous hydrodynamic fluid. We have to emphasize that the above alternative mechanism of the local current vortex does not imply that the previous conclusion obtained from the hydrodynamics is incorrect, but only an important supplement, because the model and the sample size used here are quite different.

Next, we propose two experimental methods to verify the existence of vortex in ballistic regime by tuning the strength of the external Rashba effect λ_R : the variations of the negative value of R_{NL} and the breakdown of the nonlocal WF law. Since the ee interaction dominated system is relatively insensitive to the Rashba effect, these two methods can, in principle, be used to distinguish the physics in the ballistic and viscous systems as well. Moreover, since the vortex always leads to the existence of a

magnetic flux, this exotic vortex could also be detected with the newly developed superconducting quantum interference device (SQUID)³⁵.

Finally and notably, based on a comparison between our graphene system and a square lattice model, a discussion is made that the unique linear spectrum of graphene results in a sufficient long l_e , which makes the system easier to enter into the ballistic regime. Furthermore, the exotic vortex directly originates from this ballistic transport and the consequent collisions between the flowing current and the boundaries.

ACKNOWLEDGMENTS

We thank the insightful discussions with Qing-feng Sun and Jie Liu. This work was financially supported by the Science Challenge Project (SCP) under Grant No. TZ2016003-1, NSFC under Grants Nos. 11704348, 11534001, 11822407, 11674028, and NBRPC under Grants Nos. 2017YFA0303301, 2017YFA0303304.

* jianghuaphy@suda.edu.cn

- ¹ M. E. Huber, N. C. Koshnick, H. Bluhm, L. J. Archuleta, T. Azua, P. G. Björnsson, B. W. Gardner, S. T. Halloran, E. A. Lucero, and K. A. Moler, *Rev. Sci. Instrum.* **79**, 053704 (2008).
- ² D. A. Abanin, S. V. Morozov, L. A. Ponomarenko, R. V. Gorbachev, A. S. Mayorov, M. I. Katsnelson, K. Watanabe, T. Taniguchi, K. S. Novoselov, L. S. Levitov, and A. K. Geim, *Science* **332**, 328 (2011).
- ³ J. Balakrishnan, G. K. Koon, M. Jaiswal, A. H. Castro Neto, and B. Özyilmaz, *Nat. Phys.* **9**, 284 (2013).
- ⁴ K. C. Nowack, E. M. Spanton, M. Baenninger, M. König, J. R. Kirtley, B. Kalisky, C. Ames, P. Leubner, C. Brüne, H. Buhmann, L. W. Molenkamp, D. Goldhaber-Gordaon, and K. A. Moler, *Nat. Mater.* **12**, 787 (2013).
- ⁵ R. V. Gorbachev, J. C. W. Song, G. L. Yu, A. V. Kretinin, F. Withers, Y. Cao, A. Mishchenko, I. V. Grigorieva, K. S. Novoselov, L. S. Levitov, and A. K. Geim, *Science* **346**, 448 (2014).
- ⁶ Y. Shimazaki, M. Yamamoto, I. V. Borzenets, K. Watanabe, T. Taniguchi, and S. Tarucha, *Nat. Phys.* **11**, 1032-1036 (2015).
- ⁷ M. Sui, G. Chen, L. Ma, W. Shan, D. Tian, K. Watanabe, T. Taniguchi, X. Jin, W. Yao, D. Xiao, and Y. Zhang, *Nat. Phys.* **11**, 1027-1031 (2015).
- ⁸ M. Yamamoto, Y. Shimazaki, I. V. Borzenets, and S. Tarucha, *J. Phys. Soc. Jpn* **84**, 121006 (2015).
- ⁹ D. A. Bandurin, I. Torre, R. Krishna Kumar, M. Ben Shalom, A. Tomadin, A. Principi, G. H. Auton, E. Khestanova, K. S. Novoselov, I. V. Grigorieva, L. A. Ponomarenko, A. K. Geim, and M. Polini, *Science* **351**, 1055 (2016).
- ¹⁰ D. A. Bandurin, A. V. Shytov, L. S. Levitov, R. K. Kumar, A. I. Berdyugin, M. B. Shalom, I. V. Grigorieva, A. K. Geim, and G. Falkovich, *Nat. Commun.* **9**, 4533 (2018).
- ¹¹ B. A. Braem, F. M. D. Pellegrino, A. Principi, M. Roosli, C. Gold, S. Hennel, J. V. Koski, M. Berl, W. Dietsche, W. Wegscheider, M. Polini, T. Ihn, and K. Ensslin, *Phys. Rev. B* **98**, 241304(R) (2018).
- ¹² Y. Wu, L. Zhang, C. Li, Z. Zhang, S. Liu, Z. Liao, and D. Yu, *Adv. Mater.* **30**, 1707547 (2018).
- ¹³ A. I. Berdyugin, S. G. Xu, F. M. D. Pellegrino, R. Krishna Kumar, A. Principi, I. Tórré, M. Ben Shalom, T. Taniguchi, K. Watanabe, I. V. Grigorieva, M. Polini, A. K. Geim, and D. A. Bandurin, *Science* **364**, 162 (2019).
- ¹⁴ L. Levitov, and G. Falkovich, *Nat. Phys.* **12**, 672 (2016).
- ¹⁵ P. S. Alekseev, *Phys. Rev. Lett.* **117**, 166601 (2016).
- ¹⁶ A. D. Levin, G. M. Gusev, E. V. Levinson, Z. D. Kvon, and A. K. Bakarov, *Phys. Rev. B* **97**, 245308 (2018).
- ¹⁷ A. Shytov, J. F. Kong, G. Falkovich, and L. Levitov, *Phys. Rev. Lett.* **121**, 176805 (2018).
- ¹⁸ Z. Wang, H. Liu, H. Jiang, and X. C. Xie, *Phys. Rev. B* **94**, 035409 (2016).
- ¹⁹ D. Van Tuan, J. M. Marmolejo-Tejada, X. Waintal, B. K. Nikolic, S. O. Valenzuela and S. Roche, *Phys. Rev. Lett.* **117**, 176602 (2016).
- ²⁰ M. Chandra, G. Kataria, D. Sahdev, and R. Sundararaman, *Phys. Rev. B* **99**, 165409 (2019).
- ²¹ C. Huang, Y. D. Chong, and M. A. Cazalilla, *Phys. Rev. Lett.* **119**, 136804 (2017).
- ²² P. Gallagher, C. Yang, T. Lyu, F. Tian, R. Kou, H. Zhang, K. Watanabe, T. Taniguchi, and F. Wang, *Science* **364**, 158 (2019).
- ²³ M. J. M. de Jong, and L. W. Molenkamp, *Phys. Rev. B* **51**, 13389 (1995).
- ²⁴ T. Scaffidi, N. Nandi, B. Schmidt, A. P. Mackenzie, and J. E. Moore, *Phys. Rev. Lett.* **118**, 226601 (2017).
- ²⁵ A. Lucas, and K. C. Fong, *J. Phys.: Condens. Matter* **30**, 053001 (2018).
- ²⁶ J. Crossno, J. K. Shi, K. Wang, X. Liu, A. Harzheim, A. Lucas, S. Sachdev, P. Kim, T. Taniguchi, K. Watanabe, T. A. Ohki, and K. C. Fong, *Science* **351**, 1058 (2016).
- ²⁷ The calculation process is actually based on a six-terminal system. That is to say, there exist additional two leads at the left and right side of the center region, marked by lead L and lead R, because the definitions of R_L and R_{NL} in some experiments require these two leads. However, the deductions of $R_{L,NL}$ and $\Theta_{L,NL}$ in our paper need no information from lead L and lead R, and we just assume the both the electrical and the thermal current flowing through lead L and lead R is zero. Therefore, we claim that it is a four-terminal system that we use for simplicity.
- ²⁸ The ee collision mean free path l_{ee} is usually on the order of $100nm$ in graphene. Thus, this system definitely lies in the ballistic regime no matter whether the ee interaction exists or not in Eq.1.
- ²⁹ A.-P. Jauho, N. S. Wingreen, and Y. Meir, *Phys. Rev. B* **50**, 5528 (1994).
- ³⁰ H. Jiang, L. Wang, Q. Sun, and X. C. Xie, *Phys. Rev. B* **80**, 165316 (2009).
- ³¹ *Electronic Transport in Mesoscopic Systems*, edited by S. Datta (Cambridge University Press, Cambridge, England, 1995).
- ³² We strongly suggest the readers to zoom in Fig.2 and Fig.4

on a computer screen for the convenience to read the vortex clearly. These two figures have sufficiently high DPI.

- ³³ Actually, the vortex strength can not be well defined in the ballistic regime. However, since the vortex is composite by a series of arrows arranging in a counter-clockwise line, the vortex strength can be approximately estimated with the size of these counter-clockwise arrows. Thus, from now on, we take the phrase “vortex strength” to represent the

“local-current strength in the vortex” for simplicity.

- ³⁴ J. Liu, Q. Sun, and X. C. Xie, Phys. Rev. B **81**, 245323 (2010).
³⁵ J. R. Kirtley, M. B. Ketchen, K. G. Stawiasz, J. Z. Sun, W. J. Gallagher, S. H. Blanton, and S. J. Wind, Appl. Phys. Lett. **66**, 1138 (1995).